

Photoexcited in situ loading of Pt clusters onto rGO-immobilized SnO with excellent catalytic performance toward methanol oxidation

Authors: Wu Shouliang

Date: 2017-08-15T00:00:00+00:00

Abstract

Great effort is made to maximize the surface area and expose active sites of a catalyst by distributing it over a suitable electronic conducting support. We present a design and eco-friendly construction of a two-dimensional Pt/SnO₂/reduced-graphene-oxide (rGO) nanocomposite to study the strong metal-semiconductor-support interactions as candidate highly active and durable electrocatalyst. Distinctively, highly reactive SnO_x nanoparticles (NPs) induced by laser ablation in liquids were used as a precursor to transform the graphene oxide (GO). Simultaneously, the initial amorphous-like SnO_x further crystallized into SnO₂ NPs, which were uniformly anchored onto rGO sheets. Afterward, the photoexcited electrons from semiconductor SnO₂ were used as green reducing agents. Ultrafine Pt NPs with an average size of about 1-2 nm were in situ reduced and uniformly anchored on the surface of crystallized SnO₂ NPs. Compared with the Pt/rGO catalysts without SnO₂ modification, the prepared Pt/SnO₂/rGO catalysts not only show larger electrochemical active surface area and higher catalytic activity toward methanol oxidation but also exhibit better tolerance toward CO and long-term cycle stability. The significantly enhanced electrochemical performance should be attributed to the uniformly dispersed Pt NPs with ultrafine size and the synergetic effect from the hybrid noble metal-semiconductor-carbon network components, which possess promising potential applications as electrocatalysts for methanol oxidation.

Full Text

Preamble

Photo-Excited In Situ Loading of Pt Clusters onto rGO-Immobilized SnO with Excellent Catalytic Performance toward Methanol Oxidation

Shouliang Wu ^a, Jun Liu ^a, Dewei Liang ^{a,b}, Hongmei Sun ^{a,b}, Yixing Ye ^a, Zhenfei Tian ^a, and Changhao Liang ^{a,b,*}

^a Key Laboratory of Materials Physics and Anhui Key Laboratory of Nanomaterials and Nanotechnology, Institute of Solid State Physics, Chinese Academy of Sciences, Hefei 230031, China

^b Hefei National Laboratory for Physical Sciences at the Microscale, University of Science and Technology of China, Hefei 230026, China

*Corresponding author. Tel: +86 551 65591129; Fax: +86 551 65591434; E-mail: chliang@issp.ac.cn (C.H. Liang)

Abstract

Great efforts have been made to maximize the surface area and expose active sites of catalysts by distributing them over suitable electronically conductive supports. Here we present an eco-friendly design for constructing two-dimensional Pt/SnO₂/reduced-graphene-oxide (rGO) nanocomposites (NCs) to investigate strong metal-semiconductor-support interactions as candidate highly active and durable electrocatalysts. Distinctively, highly reactive SnO₂ nanoparticles (NPs) induced by laser ablation in liquids were employed as precursors to transform graphene oxide (GO). Simultaneously, the initially amorphous-like SnO₂ further crystallized into SnO₂ NPs, which were uniformly anchored onto rGO sheets. Subsequently, photo-excited electrons from semiconductor SnO₂ served as green reducing agents, enabling ultrafine Pt NPs with an average size of 1-2 nm to be in situ reduced and uniformly anchored onto the surface of crystallized SnO₂ NPs.

Compared with Pt/rGO catalysts lacking SnO₂ modification, the prepared Pt/SnO₂/rGO catalysts exhibited not only larger electrochemical active surface area and higher catalytic activity toward methanol oxidation, but also superior tolerance toward CO and enhanced long-term cycle stability. The significantly improved electrochemical performance is attributed to the uniformly dispersed ultrafine Pt NPs and the synergistic effect derived from the hybrid noble metal-semiconductor-carbon network components, which hold promising potential as electrocatalysts for methanol oxidation.

KEYWORDS: Pt cluster; hybrid composite electrocatalyst; photo-excited reduction; methanol oxidation; laser ablation in liquids

Introduction

Fuel cells, particularly direct methanol fuel cells (DMFCs), have attracted considerable attention due to environmental concerns arising from fossil fuel consumption and the urgent demand for clean energy systems [1,2]. DMFCs can operate at low temperatures and offer high energy conversion efficiency, making them promising power sources for mobile and portable electronic devices [3-5]. However, their successful commercialization has been severely hampered

by high manufacturing costs, sluggish reaction kinetics of Pt-based catalysts, and poisoning of Pt catalysts by CO-like species generated during methanol oxidation [6,7].

For methanol oxidation applications, Pt catalysts with ultrafine sizes are highly desirable because they provide increased surface area and abundant corner and edge atoms. Downsizing Pt NPs thus improves catalytic activity while reducing Pt usage and manufacturing costs. Nevertheless, ultrafine Pt NPs tend to aggregate into larger species under reaction conditions due to their high surface energy, causing serious performance degradation. An effective strategy to address this deactivation involves uniformly loading catalysts onto suitable supporting materials that offer low cost, high surface area, and excellent conductivity. As a two-dimensional carbon material with a single atomic layer, graphene has recently gained increased attention as an excellent catalyst support for fuel cells [8-12]. It provides a large specific surface area for efficient catalyst dispersion, high electrical conductivity for rapid electron transfer, superior thermal and chemical stability to prevent corrosion, and a dense honeycomb crystal structure that promotes gas flow.

To improve CO poisoning tolerance of Pt catalysts, a widely accepted approach involves adding metal oxides (TiO₂, SnO₂, SiO₂, and CeO₂) as additives [13-16]. The low cost and abundance of metal oxides help reduce manufacturing expenses, while their use promotes uniform dispersion of Pt NPs, thereby increasing the active surface area per unit mass of Pt. More importantly, most metal oxides possess substantial oxygen storage and release capacity, which plays a crucial role in further oxidizing CO-like species. However, metal oxides suffer from poor electronic conductivity, making it difficult to achieve sufficient electrocatalytic properties when integrated with Pt catalysts.

To combine the excellent features of metal oxides with the outstanding electronic conductivity and large surface area of graphene, various Pt/metal-oxides/rGO NCs have been synthesized and investigated as electrocatalysts for methanol oxidation [17-20]. For example, Wang and co-workers prepared Pt/TiO₂/rGO catalysts with significantly enhanced catalytic activity and stability [17], while Geng's group demonstrated that Pt/CeO₂/rGO catalysts exhibited lower overpotential, much higher catalytic activity, and improved stability compared with Pt/rGO catalysts [18]. However, most synthetic methods employed sodium borohydride or hydrazine hydrate as reducing agents, which are highly toxic and pose serious environmental and health risks, limiting their practical applicability. Additionally, surfactants such as polyvinylpyrrolidone (PVP) are typically introduced as stabilizers to control particle growth, but these can be strongly adsorbed on Pt catalyst surfaces and severely affect catalytic performance. More importantly, because graphene has higher surface area and adsorbability, a large proportion of Pt precursor associates with graphene rather than metal oxides, causing many reduced Pt catalysts to disperse only on graphene surfaces without effectively attaching to metal oxides.

We propose a simple and green strategy to fabricate two-dimensional

Pt/SnO /rGO hybrid nanocomposites based on laser ablation in liquids (LAL) combined with a facile photo-assisted in situ reduction method. This approach offers several advantages: (i) photo-excited electrons from SnO NPs serve as clean reducing agents without introducing organic surfactants throughout the synthesis; (ii) Pt reduction occurs on the SnO surface, leading to ultrafine Pt NPs being in situ anchored onto SnO NPs; (iii) the method successfully produces ultrafine Pt NPs averaging 1-2 nm that are evenly distributed on SnO surfaces; and (iv) the as-prepared Pt/SnO /rGO catalysts demonstrate higher catalytic activity and better long-term performance toward methanol oxidation compared with Pt/rGO catalysts.

Experimental

2.1 Chemical Reagents and Materials

All reagents used in the experiments were of analytical grade and applied without further purification. Graphite powder was purchased from Tianjin Guangfu Fine Chemical Research Institute. GO was synthesized from graphite using a modified Hummers method [21,22]. Double-distilled water (resistance $>18 \text{ M}\Omega \cdot \text{cm}^{-1}$) was used throughout all experiments.

2.2 LAL-Assisted Preparation of SnO /rGO NCs

Highly dispersed SnO NPs decorated on rGO sheets were first prepared according to our previous report [23]. Briefly, a polished tin plate (99.99% purity) was fixed in a vessel containing 15 mL deionized water and ablated for 5 minutes using a fundamental Nd:YAG laser (1064 nm) with a pulse repetition rate of 10 Hz, pulse duration of 10 ns, and laser energy of 80 mJ per pulse. After ablation, the obtained fresh colloidal solution was quickly mixed with 2 mL GO solution ($8 \times 10^{-3} \text{ g/mL}$) and placed inside a dark chamber. One week later, the newly prepared SnO /rGO NCs were collected by centrifugation.

2.3 Photo-Assisted In Situ Reduction Route for Pt/SnO /rGO NCs

Ultrafine Pt NPs were in situ reduced under UV-light irradiation. Prior to irradiation, the SnO /rGO precipitates and 2 mL chloroplatinic acid (H PtCl_6 , 4 mg/mL) were added to a 50 mL test tube containing 30 mL deionized water. After ultrasonic treatment for 10 minutes, the mixture was illuminated by a 300 W mercury lamp at room temperature for 90 minutes at a distance of 40 cm. The black precipitates were collected by centrifugation and washed with deionized water three times. Final products were obtained by drying the precipitates at $50 \text{ }^\circ\text{C}$ in a vacuum-drying box. By adjusting the amount of added H PtCl_6 solution (1, 2, and 3.5 mL) while keeping other parameters constant, a series of catalysts with different mass ratios of Pt and SnO were obtained and denoted as Pt . /SnO /rGO, Pt . /SnO /rGO, and Pt . /SnO /rGO, respectively. The mass ratios were determined by inductively coupled plasma atomic emission spectroscopy (ICP-AES).

2.4 Preparation of Pt/rGO NCs

For comparison, Pt/rGO NCs were synthesized using a chemical method modified from other reports [24,25]. In a typical synthesis, 0.6 mL H PtCl solution (4 mg/mL) and 0.2 mL formic acid (HCOOH) were added to 15 mL GO solution (8×10^{-3} g/mL). After ultrasonic treatment for 30 minutes, the suspension was stored at room temperature for 48 hours. Finally, the precipitates were washed with deionized water three times and dried at 50 °C in a vacuum-drying box.

2.5 Structure Characterization

The surface chemical constituents of prepared catalysts were analyzed by X-ray photoelectron spectroscopy (XPS, Thermo ESCALAB 250). Transmission electron microscopy (TEM) images were captured on a JEOL-2010 apparatus with 200 kV accelerating voltage. High-angle annular dark-field scanning transmission electron microscopy (HAADF-STEM) images were recorded on a JEM-ARM-200F instrument (University of Science and Technology of China). Before TEM examination, products were ultrasonically dispersed in ethanol, and a drop of suspension was deposited onto a Cu grid coated with a thin carbon film.

2.6 Electrochemical Measurements

All electrochemical measurements were performed on a standard three-electrode Zahner IM6e electrochemical workstation. A Pt wire and a KCl-saturated Ag/AgCl electrode served as counter and reference electrodes, respectively. A glassy carbon (GC) electrode (3 mm diameter) was polished to a mirror finish with Al₂O₃ slurry (0.3 μm) and ultrasonically cleaned in ethanol for several minutes. Subsequently, 10 μL of as-prepared catalyst suspension was directly pipetted onto the working electrode, followed by solvent evaporation at room temperature. Exactly 20 μL of Nafion solution was then dropped onto the dried sample. The Pt weight on each working electrode was calculated through ICP measurement. A 0.5 M NaOH-saturated H₂SO₄ aqueous solution was used as electrolyte for measuring electrochemical active surface area (ECSA). Cyclic voltammetry (CV) measurements for evaluating methanol oxidation performance were performed at 50 mV · s⁻¹ in a mixed solution of 0.5 M H₂SO₄ and 0.5 M CH₃OH. Current-time (CA) curves were recorded at a constant potential of 0.615 V for 60 minutes in 0.5 M H₂SO₄ containing 0.5 M CH₃OH. To further assess catalyst stability, long-term CV tests (1200 cycles) were conducted from 0 to 1 V at 50 mV · s⁻¹.

Results and Discussion

3.1 Strategy for Synthesizing Pt/SnO₂/rGO NCs

Scheme 1. Illustration for the synthesis of Pt/SnO₂/rGO NCs.

We propose the following formation mechanism for Pt/SnO₂/rGO NCs in our synthesis strategy. In previous reports, we have repeatedly demonstrated that

most fresh colloids generated by LAL possess high activity and reactivity [26–28]. In the present work, LAL-induced fresh SnO₂ colloids exhibiting a low valence state of Sn cations and poor crystallization were first dispersed on GO sheets. After aging treatment at room temperature, GO sheets evolved in situ into rGO sheets, while the poorly crystalline SnO₂ NPs simultaneously converted into well-crystallized SnO₂ NPs uniformly distributed on rGO sheets, as shown in Figure S1. The high distribution of SnO₂ NPs on rGO sheets is expected to result in high dispersion of Pt catalysts. Scheme 1 illustrates the synthesis process of Pt/SnO₂/rGO NCs. Under UV-light irradiation, photo-excited electrons migrated from the valence band of SnO₂ NPs to the conduction band, leaving holes in the valence band. PtCl₄²⁻ adsorbed on SnO₂ surfaces was then in situ reduced to Pt atoms by the photo-excited electrons. Numerous reduced Pt atoms subsequently aggregated into ultrafine Pt NPs uniformly anchored on SnO₂ surfaces. This reduction mechanism can be expressed by the following formulas:

- (a) Adsorption of PtCl₄²⁻ on SnO₂ surface:

$$\text{PtCl}_4^{2-} + \text{SnO}_2 \rightarrow \text{SnO}_2\text{-(PtCl}_4^{2-})_{\text{ads}}$$
- (b) Creation of electron-hole pairs:

$$\text{SnO}_2 + h\nu \rightarrow \text{SnO}_2(e^- + h^+)$$
- (c) Reduction of ultrafine Pt NPs:

$$\text{SnO}_2\text{-(PtCl}_4^{2-})_{\text{ads}} + ne^- \rightarrow \text{SnO}_2\text{-Pt(NPs)} + \text{Cl}^-$$

3.2 Characterization of the Prepared Pt/SnO₂/rGO NCs

Figure 1 [Figure 1: see original paper]. Representative (a) TEM, (b,c) HAADF-STEM images, and (d) EDS mapping of the prepared Pt/SnO₂/rGO NCs; (b, inset) particle size distribution histogram of Pt NPs.

The morphology of as-synthesized Pt/SnO₂/rGO NCs was characterized by TEM and HAADF-STEM. The low-magnification TEM image (Figure 1a) shows large quantities of small NPs uniformly dispersed on rGO sheets. Figures 1b and 1c display representative HAADF-STEM images, where ultrafine Pt NPs with an average size of 1.4 (±0.4) nm (inset of Figure 1b) were homogeneously dispersed on SnO₂ NP surfaces without noticeable agglomeration. The EDS mapping (Figure 1d) of the as-prepared ternary hybrid clearly demonstrates uniform distribution of all elements including Sn, O, Pt, and C. Notably, Pt NPs remained firmly and uniformly anchored on SnO₂ support even after prolonged strong sonication, indicating strong interactions between Pt and SnO₂ NPs. Therefore, rGO sheets play a crucial role in preventing aggregation of Pt or SnO₂ NPs. Conversely, the highly dispersed small NPs anchored on rGO surfaces can act as “spacers” to prevent rGO sheet overlapping.

Figure 2 [Figure 2: see original paper]. High-resolution XPS spectra obtained from the as-prepared Pt/SnO₂/rGO NCs: (a) Sn 3d, (b) Pt 4f, and (c) C 1s; (d) high-resolution C 1s XPS spectra of GO.

XPS was employed to analyze the chemical states of elements in Pt . /SnO /rGO NCs. As shown in Figure 2a, binding energies at 487.2 and 495.5 eV indicate that Sn exists in the Sn oxidation state [29]. In the Pt 4f XPS spectra (Figure 2b), peaks at 71.2 eV and 74.5 eV are assigned to Pt(0), while signals at 72.2 and 75.6 eV correspond to Pt in the +2 state [15]. Figure 2c displays high-resolution C 1s XPS spectra, which can be divided into three peaks corresponding to carbon atoms in different oxygen-containing functional groups. The peak at 284.73 eV is assigned to C-C bonds, while peaks at 286.48 and 288.67 eV correspond to C-O and C=O bonds, respectively, showing much weaker intensity compared with the C-C peak. Comparison with high-resolution C 1s XPS spectra from GO (Figure 2d) reveals dramatically decreased peak intensities of oxygen-containing functional groups, confirming GO reduction to rGO [30]. These results demonstrate successful synthesis of Pt/SnO /rGO NCs via the photo-assisted in situ reduction process.

Figure 3 [Figure 3: see original paper]. Effects of H PtCl concentration on catalyst morphology. Regardless of H PtCl concentration changes, ultrafine Pt NPs were successfully assembled and closely adhered to SnO supports without extensive aggregation. Both Pt coverage density and NP size increased with Pt loading amount. More than 200 Pt NPs were randomly selected to determine size distribution histograms. Pt NPs in Pt . /SnO /rGO catalysts (inset of Figure 3b) averaged 1.2 (± 0.4) nm, while those in Pt . /SnO /rGO catalysts (inset of Figure 3e) were about 1.7 (± 0.5) nm. Figures S2a and S2b show EDS mapping of Pt . /SnO /rGO and Pt . /SnO /rGO catalysts, respectively. Both catalysts contained four uniformly dispersed elements (Sn, O, Pt, and C), indicating uniform dispersion of Pt and SnO NPs on rGO sheets. Overall, using photo-excited electrons as reducing agents enables preparation of a series of Pt/SnO /rGO catalysts with different Pt/SnO mass ratios by adjusting H PtCl feedstock concentration.

3.3 Electrochemical Properties of the Prepared Catalysts

To evaluate the potential application of as-prepared Pt/SnO /rGO NCs, we investigated their electrochemical properties for methanol oxidation in acidic media. For comparison, electrochemical measurements were also performed on Pt/rGO catalysts prepared under identical conditions, where multiple Pt NPs with an average size of 3.5 (± 1.2) nm were attached to rGO sheets (Figure S3).

Figure 4 [Figure 4: see original paper]. CV curves of GC electrodes modified with prepared catalysts measured at 50 $\text{mV} \cdot \text{s}^{-1}$ in (a) 0.5 M N -saturated H SO and (b) 0.5 M H SO + 0.5 M CH OH; CA curves of prepared catalysts measured in 0.5 M H SO + 0.5 M CH OH at a constant potential of 0.615 V.

Table 1 . Electrocatalytic properties of different catalysts

Catalyst	ECSA (cm ² /mg Pt)	Mass activity (mA/mg Pt)	Forward peak potential (V)	If/I _b
Pt . /SnO ₇ /rGO	759.8	-	-	-
Pt . /SnO ₈ /rGO	805.6	638.3	0.615	-
Pt . /SnO ₆ /rGO	649.2	-	-	-
Pt/rGO	562.0	368.6	0.699	-

Electrochemical active surface area (ECSA), which is proportional to the true surface area of Pt catalysts, represents a critical factor determining catalytic activity. ECSA was investigated by CV from -0.2 to 1 V at 50 mV · s⁻¹ in 0.5 M N₂-saturated H₂SO₄ aqueous solution (Figure 4a). Typical hydrogen adsorption/desorption was observed between -0.2 V and 0.12 V (vs. Ag/AgCl). ECSA values were calculated from hydrogen adsorption area using the equation:

$$\text{ECSA} = Q_{\text{H}} / (0.21 \times [\text{Pt}])$$

where Q_{H} (in mC · cm⁻²) is the charge exchanged during electro-desorption of hydrogen atoms on Pt, 0.21 (in mC · cm⁻²) represents the monolayer charge (calculated from a surface density of 1.3×10^{15} atoms · cm⁻²), and [Pt] (in mg · cm⁻²) is the Pt loading on the working electrode. As shown in Table 1, Pt . /SnO₇/rGO, Pt . /SnO₈/rGO, and Pt . /SnO₆/rGO catalysts exhibited ECSA values of 759.8, 805.6, and 649.2 cm² · mg⁻¹, respectively—all higher than Pt/rGO catalysts (562.0 cm² · mg⁻¹). The larger ECSA values of Pt/SnO_n/rGO catalysts result from uniform dispersion of ultrafine Pt NPs on SnO_n supports, consistent with observed morphology. These higher ECSA values provide more active sites for electrochemical reactions, offering potential for superior methanol oxidation activity.

Mass activity of Pt-based catalysts, normalized by Pt loading mass, is commonly adopted to compare catalytic activities for methanol oxidation. Figure 4b shows typical CVs of prepared catalysts measured in 0.5 M H₂SO₄ containing 0.5 M CH₃OH at 50 mV · s⁻¹. All curves exhibited two well-defined peaks in forward and backward scans. The forward scan peak corresponds to methanol oxidation, while the backward peak likely arises from oxidation of incompletely oxidized carbonaceous species formed during the forward scan. Maximum current densities and corresponding potentials were determined from Figure 4b and summarized in Table 1. Current densities followed the order: Pt . /SnO₇/rGO > Pt . /SnO₈/rGO > Pt . /SnO₆/rGO > Pt/rGO. Pt . /SnO₈/rGO catalysts displayed the highest current density of 638.3 mA · mg⁻¹, approximately 1.73 times that of Pt/rGO catalysts (368.6 mA · mg⁻¹). Another important metric, the ratio of forward (I_f) to backward (I_b) peak current densities, evaluates catalyst poisoning tolerance [33,34]. Higher I_f/I_b values indicate greater tolerance to intermediate carbon species, meaning methanol oxidizes to CO more efficiently with minimal carbonaceous residue accumulation. Calculations based on Figure 4b revealed that all Pt/SnO_n/rGO catalysts exhibited higher I_f/I_b values than Pt/rGO catalysts. Additionally, the methanol oxidation

peak potential was 0.615 V for Pt . /SnO /rGO versus 0.699 V for Pt/rGO, representing a negative shift of 0.084 V. Thus, SnO addition not only facilitated the oxygen reduction reaction but also improved CO poisoning tolerance. Specific activities of Pt/SnO /rGO catalysts were also compared with Pt/rGO (Figure S4), revealing superior specific activities for all three Pt/SnO /rGO catalysts. These results provide clear evidence for the superior electrocatalytic activity of Pt/SnO /rGO catalysts toward methanol oxidation.

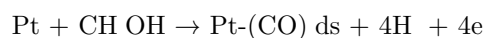
Catalyst stability was evaluated by CA curves at 0.615 V constant potential in 0.5 M H₂SO₄ containing 0.5 M CH₃OH for 3600 seconds. Figure 4c shows initial rapid current decay for all catalysts due to intermediate CO-like species formation during methanol oxidation [17]. All Pt/SnO /rGO catalysts exhibited significantly higher initial current densities and maintained higher current densities throughout the test range compared with Pt/rGO, indicating superior catalytic activity and stability. These results are consistent with CV data in Figure 4b.

Long-term stability was further demonstrated by continuous CV cycling between 0 and 1 V at 50 mV · s⁻¹ for 1200 cycles. CVs at different cycle numbers are presented in Figures 5a-d, while Figures 5e and 5f show mass activities and normalized peak current densities obtained from long-term tests. All peak current densities gradually decreased with continued cycling, likely due to intermediate species accumulation and Pt catalyst aggregation (Figure S5) during extended CV testing. As shown in Figure 5e [Figure 5: see original paper], all Pt/SnO /rGO catalysts maintained higher current densities than Pt/rGO throughout the entire test duration, further confirming their superior methanol oxidation activity. Figure 5f reveals that Pt . /SnO /rGO retained 72.4% of its initial peak current density after 1200 cycles, higher than Pt/rGO (54.5%). Pt . /SnO /rGO and Pt . /SnO /rGO displayed remaining forward peak current densities of 68.7% and 69.4%, respectively, also exceeding Pt/rGO performance. These results clearly demonstrate that all Pt/SnO /rGO catalysts possess excellent long-term stability for methanol oxidation.

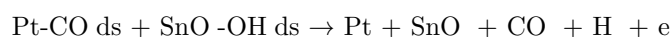
Figure 5 [Figure 5: see original paper]. CVs at different cycle numbers in 0.5 M H₂SO₄ containing 0.5 M CH₃OH at 50 mV · s⁻¹ for (a) Pt . /SnO /rGO, (b) Pt . /SnO /rGO, (c) Pt . /SnO /rGO, and (d) Pt/rGO catalysts; (e) mass activities and (f) normalized peak current densities at different cycle numbers for prepared catalysts.

The excellent performance of Pt/SnO /rGO catalysts toward methanol oxidation can be understood through several factors. First, catalyst supports with large surface area effectively prevent Pt NP coalescence, leading to formation of highly dispersed, high-density ultrafine Pt NPs. These well-dispersed ultrafine Pt NPs provide abundant electrochemically active sites, active facets, and increased active surface area. Additionally, the excellent stability of SnO₂ and graphene maintains structural integrity under harsh electrochemical conditions, while graphene' s superior conductivity enables rapid electron/charge carrier transport. Importantly, synergistic effects between Pt and SnO₂ play a crucial

role in promoting further oxidation of CO-like species during methanol oxidation, resulting in high stability and apparent anti-poisoning tolerance. During methanol oxidation, methanol molecules first adsorb on Pt surfaces and subsequently decompose to intermediate Pt-(CO) ds species. This process can be described by:



The generated CO-like species can adsorb on Pt surfaces and occupy active sites, causing rapid catalytic activity decline. With SnO₂ addition, oxygen-containing species (such as OH) are more easily formed on its surface, which facilitates oxidation of CO-like species on neighboring poisoned Pt sites and liberates Pt active sites for further methanol oxidation. The proposed reaction mechanism is [14,35]:



Electro-oxidation of CO-like species is promoted only when Pt NPs contact SnO₂. In this study, the specific photo-assisted in situ reduction method strongly anchored reduced Pt NPs on SnO₂ surfaces, resulting in better CO tolerance than Pt/rGO catalysts.

Conclusion

We have successfully designed and prepared novel Pt/SnO₂/rGO ternary hybrid electrocatalysts by uniformly anchoring ultrafine Pt NPs onto SnO₂ in contact with rGO substrates. As anode catalysts for methanol oxidation, these ternary hybrids exhibited significantly reduced overpotential, greatly enhanced catalytic activity, and notably improved long-term durability compared with conventional Pt catalysts supported on rGO sheets. This excellent performance is attributed to the ultrafine size of Pt NPs and the unique catalyst structure. Strong interactions between Pt and SnO₂ not only create a possible synergistic effect but also greatly stabilize Pt catalysts. Systematic investigation of Pt loading amounts suggests that the composition of many Pt-based catalysts could be optimized. This work provides new insights for designing and preparing hybrid materials for DMFCs and other energy conversion/storage applications.

Acknowledgments

This work was financially supported by the National Basic Research Program of China (2014CB931704) and the National Natural Science Foundation of China (NSFC, Nos. 51371166, 11504375, 11304315).

Appendix A. Supplementary Materials

Supplementary data associated with this article can be found in the online version at <http://dx.doi.org/10.1016/j.nanoen.2016.XX.XXX>.

References

- [1] J. Xie, Q.H. Zhang, L. Gu, S. Xu, P. Wang, J.G. Liu, Y. Ding, Y.F. Yao, C.W. Nan, M. Zhao, Y. You, Z.G. Zou, *Nano Energy* 21 (2016) 247-257.
- [2] R.F. Service, *Science* 296 (2002) 1222-1224.
- [3] L.G. Feng, K. Li, J.F. Chang, C.P. Liu, W. Xing, *Nano Energy* 15 (2015) 462-469.
- [4] A.C. Chen, P. Holt-Hindle, *Chem. Rev.* 110 (2010) 3767-3804.
- [5] H.J. Huang, X. Wang, *J. Mater. Chem. A* 2 (2014) 6266-6291.
- [6] W.J. Huang, H.T. Wang, J.G. Zhou, J. Wang, P.N. Duchesne, D. Muir, P. Zhang, N. Han, F.P. Zhao, M. Zeng, J. Zhong, C.H. Jin, Y.G. Li, S.T. Lee, H.J. Dai, *Nat. Commun.* 6 (2015) 1-8.
- [7] Y.Q. Huang, Y.J. Liu, Z.H. Yang, J.L. Jia, X. Li, Y. Luo, Y.P. Fang, *J. Power Sources* 246 (2014) 868-875.
- [8] L. Zhao, Z.B. Wang, J.L. Li, J.J. Zhang, X.L. Sui, L.M. Zhang, *J. Mater. Chem. A* 3 (2015) 5313-5320.
- [9] S.L. Wu, J. Liu, Z.F. Tian, Y.Y. Cai, Y.X. Ye, Q.L. Yuan, C.H. Liang, *ACS Appl. Mater. Interfaces* 7 (2015) 22935-22940.
- [10] F.H. Li, Y.Q. Guo, Y. Liu, J. Yan, W. Wang, J.P. Gao, *Carbon* 67 (2014) 617-622.
- [11] Z.F. Li, L. Xin, F. Yang, Y.D. Liu, Y.Z. Liu, H.Y. Zhang, L. Stanciu, J. Xie, *Nano Energy* 16 (2015) 281-292.
- [12] J.J. Shao, Z.J. Li, C. Zhang, L.F. Zhang, Q.H. Yang, *J. Mater. Chem. A* 2 (2014) 12431-12438.
- [13] C.Y. Zhai, M.S. Zhu, D. Bin, H.W. Wang, Y.K. Du, C.Y. Wang, P. Yang, *ACS Appl. Mater. Interfaces* 6 (2014) 17753-17761.
- [14] F. Han, X.M. Wang, J. Lian, Y.Z. Wang, *Carbon* 50 (2012) 5498-5504.
- [15] T.H.T. Vu, T.T.T. Tran, H.N.T. Le, L.T. Tran, P.H.T. Nguyen, H.T. Nguyen, N.Q. Bui, *Electrochim. Acta* 161 (2015) 335-342.
- [16] C. Feng, T. Takeuchi, M.A. Abdelkareem, T. Tsujiguchi, N. Nakagawa, *J. Power Sources* 242 (2013) 57-64.
- [17] B.Y. Xia, B. Wang, H.B. Wu, Z.L. Liu, X. Wang, X.W. Lou, *J. Mater. Chem.* 22 (2012) 16499-16505.
- [18] X. Yu, L. Kuai, B.Y. Geng, *Nanoscale* 4 (2012) 5738-5743.
- [19] L.T. Ye, Z.S. Li, X.F. Zhang, F.L. Lei, S. Lin, *J. Mater. Chem. A* 2 (2014) 8545-8551.
- [20] X. Wang, X.Y. Li, D.P. Liu, S.Y. Song, H.J. Zhang, *Chem. Commun.* 48 (2012) 11724-11726.
- [21] W.S. Hummers Jr, R.E. Offeman, *J. Am. Chem. Soc.* 80 (1958) 1339.
- [22] Y.X. Xu, H. Bai, G.W. Lu, C. Li, G.Q. Shi, *J. Am. Chem. Soc.* 130 (2008) 5856-5857.
- [23] Y.X. Ye, P.P. Wang, E.M. Dai, J. Liu, Z.F. Tian, C.H. Liang, G.S. Shao, *Phys. Chem. Chem. Phys.* 16 (2014) 8801-8807.
- [24] S.H. Sun, F. Jaouen, J.P. Dodelet, *Adv. Mater.* 20 (2008) 3900-3904.
- [25] R.Y. Wang, D.C. Higgins, M.A. Hoque, D.U. Lee, F. Hassan, Z.W. Chen, *Scientific Reports* 3 (2013) 1-7.

- [26] Z.F. Tian, C.H. Liang, J. Liu, H.M. Zhang, L.D. Zhang, *J. Mater. Chem.* 21 (2011) 18242-18247.
- [27] Z.F. Tian, C.H. Liang, J. Liu, H.M. Zhang, L.D. Zhang, *J. Mater. Chem.* 22 (2012) 17210-17214.
- [28] J. Liu, Y.Y. Cai, Z.F. Tian, G.S. Ruan, Y.X. Ye, C.H. Liang, G.S. Shao, *Nano Energy* 9 (2014) 282-290.
- [29] H.J. Wang, F.Q. Sun, Y. Zhang, L.S. Li, H.Y. Chen, Q.S. Wu, J.C. Yu, *J. Mater. Chem.* 20 (2010) 5641-5645.
- [30] Y.M. Sun, X.L. Hu, W. Luo, Y.H. Huang, *ACS Nano* 5 (2011) 7100-7107.
- [31] Z. Qiu, H. Huang, J. Du, T. Feng, W.K. Zhang, Y.P. Gan, X.Y. Tao, *J. Phys. Chem. C* 117 (2013) 13770-13775.
- [32] S. Anandan, A. Manivel, M. Ashokkumar, *Fuel Cells* 6 (2012) 956-962.
- [33] L.X. Ding, A.L. Wang, G.R. Li, Z.Q. Liu, W.X. Zhao, C.Y. Su, Y.X. Tong, *J. Am. Chem. Soc.* 134 (2012) 5730-5733.
- [34] Y.F. Hao, Y.Y. Yang, L.J. Hong, J.H. Yuan, L. Niu, Y.H. Gui, *ACS Appl. Mater. Interfaces* 6 (2014) 21986-21994.
- [35] F. Ye, J.J. Li, T.T. Wang, Y. Liu, H.J. Wei, J.L. Li, X.D. Wang, *J. Phys. Chem. C* 112 (2008) 12894-12898.

Note: Figure translations are in progress. See original paper for figures.

Source: ChinaXiv – Machine translation. Verify with original.